Improved recursive algorithm for light scattering by a multilayered sphere

Wen Yang

An improved recurrence algorithm to calculate the scattering field of a multilayered sphere is developed. The internal and external electromagnetic fields are expressed as a superposition of inward and outward waves. The alternative yet equivalent expansions of fields are proposed by use of the first kind of Bessel function and the first kind of Hankel function instead of the first and the second kinds of Bessel function. The final recursive expressions are similar in form to those of Mie theory for a homogeneous sphere and are proved to be more concise and convenient than earlier forms. The new algorithm avoids the numerical difficulties, which give rise to significant errors encountered in practice by previous methods, especially for large, highly absorbing thin shells. Various calculations and tests show that this algorithm is efficient, numerically stable, and accurate for a large range of size parameters and refractive indices.

OCIS codes: 290.4210, 290.5850, 290.1310, 010.1110.

1. Introduction

The electromagnetic (EM) scattering by a multilayered sphere has many significant applications.[1] Light absorption by aerosols has a heating effect in the atmosphere, which contrasts with the cooling effect of nonabsorptive particles. The balance between the cooling and the heating effects depends on the absorption and scattering properties of the particles. Also, the same amount of absorbing aerosols for different types of mixture may result in fairly different climate effects.[2,3] For the water-soluble aerosol, virtually most of the calculations have assigned a volume-average refractive index to the aerosol (e.g., the growth of the tropospheric water-soluble aerosol with humidity). However, when the aerosol is water insoluble, we cannot assign it a volume-average refractive index; if this is done, the fact that the liquid is adsorbed on the surface will be neglected.[4] In fact, particles found in nature are frequently not homogeneous in composition but sometimes exhibit a layered or radially stratified structure or other inhomogeneous structures.[3] In light of this, it is important to be able to calculate the scattering field for a multilayered sphere.[4]

The theory of EM scattering from a coated sphere was first worked out by Aden and Kerker many years ago.[5] Many subsequent computations were based on their method. Fenn and Oser[6] applied this model and considered the scattering properties of a concentric soot–water sphere. Bohren and Huffman[7] also described the procedure of scattering by a coated sphere and, furthermore, attached a calculation code to this question. However, this code, as expressed by them, should not be used for a large and strongly absorbing sphere. Although the formulation is conceptually simple and straightforward, the computation still suffers from several defects. Numerical inaccuracies can develop because of round-off errors, and some of the calculated quantities can become so large as to cause computer overflow. To circumvent these various difficulties, Toon and Ackerman[8] recast the conventional expressions for a single-layered sphere in a form amenable to accurate calculations. Unfortunately, their expressions can be applied only to a single-layered sphere. Bhandari[9] proposed a complete set of scattering coefficients for a multilayered sphere. The calculation procedure is based on a prescription that relates the scattering coefficients for a l-layered sphere to those for a $(l - 1)$-layered sphere. The deducing procedure, frankly speaking, is long-winded, and the expressions are also a little bit complicated. Theoretically, a computer program

The author (ywen@ns.lzb.ac.cn) is with the Cold and Arid Regions Environmental and Engineering Research Institute, Chinese Academy of Sciences, 260 Dong Gang West Road, Lanzhou, 730000 Gansu Province, China.

Received 8 June 2002; revised manuscript received 8 November 2002.

0003-6935/03/091710-11$15.00/0

for the scattering of a multilayered sphere is not inconceivable.[9] Practically, it could be difficult for more than four or five layers. At the same time, the above two methods also encountered the round-off errors when one deals with the large nonabsorbing sphere.

Recently Wu and Wang[10] first developed an elegant recursive method. After that, Wu *et al.*[11] presented an improved algorithm for a plane wave or a Gaussian beam. This algorithm is concise in form and more stable for computing the scattering coefficients. Johnson[12] also developed a recurrence algorithm with a somewhat different form. However, the computational difficulties were still encountered in practice, more specifically, for the case of a thin, strongly absorbing shell. Mackowski *et al.*[13] implemented different recursive formulas to estimate the thermal behavior of particles. But Kai and Massoli[14] found that Mackowski *et al.*'s method cannot perform the calculation for a finely stratified sphere because of the round-off errors introduced by the ratios of the Riccati–Bessel functions. To overcome the round-off errors for a finely stratified sphere, Kai and Massoli[14] presented a new approach for the calculation of ratios of Riccati–Bessel functions by using the Taylor expansion. Actually, as pointed out by Wu *et al.*,[11] we do not require a Taylor expansion of the ratios of Riccati–Bessel functions if a modified algorithm is used. Even though a number of authors have contributed to extend the computable region, the earlier methods, as mentioned above, are still subject to various computational difficulties. In this paper the primary objective is to present a more concise and numerically stable expression for a multilayered sphere with an arbitrary number of layers on top of the core.

In Section 2 the EM fields inside the sphere are first considered a superposition of two kinds of wave: inward and outward waves. A new set of scattering coefficients is derived for a multilayered sphere. In Section 3 a numerically stable and concise recursive algorithm, which is not subject to round-off errors and the numerical overflow associated with the computation of Riccati–Bessel functions of large complex arguments, is described for calculation of the scattering fields. We also present the computational schemes for calculating the logarithmic derivatives and the ratio of the Riccati–Bessel function and illustrate the numerical stability of these schemes. Section 4 is devoted to various calculations and tests, which show that the expressions are simple and suitable for computer coding, and the results are numerically stable and accurate.

2. Scattering Coefficients

The particle illuminated by plane EM waves is assumed to be composed of a series of concentric spheres (Fig. 1). Each is characterized by a size parameter $x_l = 2\pi N r_l/\lambda = k r_l$ and a relative refractive index $m_l = N_l/N = n_l + ik_l$, $l = 1, 2, \ldots, L$, where λ is the wavelength of the incident wave, r_l is the outer radius of the lth layer, N and N_l are the refractive

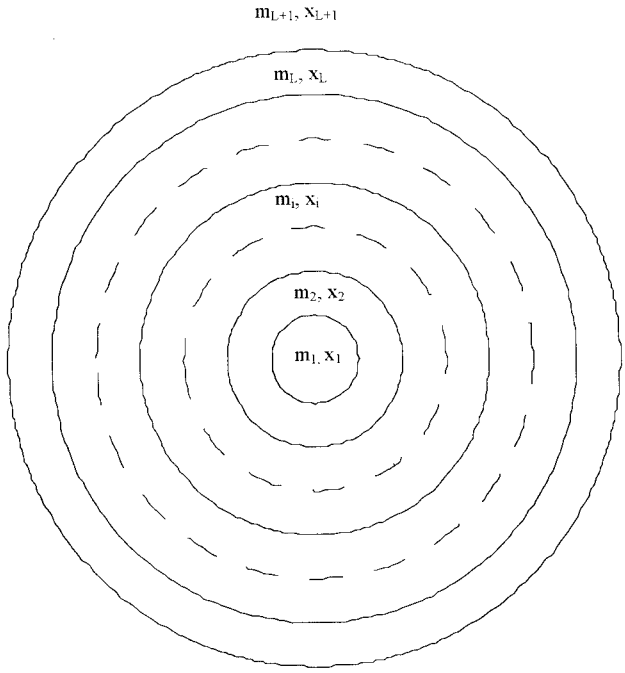

Fig. 1. Geometry of the scattering problem by a multilayered sphere.

indices of the medium outside the particle and lth component, and k is the propagation constant. In the region outside the particle, the relative refractive index is $m_{L+1} = 1$. The magnetic permeability is assumed to have the free-space value $\mu = \mu_0$ everywhere. Suppose the incident electric field is an x-polarized wave, $\mathbf{E}_i = E_0 \exp(ikr \cos\theta)\hat{\mathbf{e}}_x$. The total space is then divided into two regions: One is the region inside the multilayered sphere, and the other is the surrounding medium outside the particle. Let us first consider the case of an illuminating plane wave with a time-harmonic factor $\exp(-i\varpi t)$. In the total space (inside and outside the sphere), the E, M fields are considered a superposition of two kinds of wave: inward and outward waves from a physical point of view. The direction of propagation of these wave fronts is inward when the radial dependence is governed by the first kind of spherical Bessel function $j_n(kr)$ and outward when it is governed by the first kind of spherical Hankel function $h_n^{(1)}(kr)$.[15] For example, the electric field intensities of inward and outward waves, $\mathbf{E}_{\text{in}}$ and $\mathbf{E}_{\text{out}}$, are expressed in terms of complex spherical eigenvectors,

$$\mathbf{E}_{\text{in}} = \sum_{n=1}^{\infty} E_n [c_n^{(l)} \mathbf{M}_{o1n}^{(1)} - i d_n^{(l)} \mathbf{N}_{e1n}^{(1)}]$$

and

$$\mathbf{E}_{\text{out}} = \sum_{n=1}^{\infty} E_n [i a_n^{(l)} \mathbf{N}_{e1n}^{(3)} - b_n^{(l)} \mathbf{M}_{o1n}^{(3)}],$$

respectively. This improvement not only makes the expansions similar to those obtained from Mie theory for a single sphere but also avoids some of the numerical difficulties. It should be noted here that we

used only the first kind of Bessel function and the first kind of Hankel function. The choice is different from the choice of the first and the second kinds of Bessel function in the traditional, earlier expressions in some degree.[7,10,13] As a consequence, the expansions of the fields in the lth region are given by

$$\mathbf{E}_l = \sum_{n=1}^{\infty} E_n[c_n^{(l)}\mathbf{M}_{o1n}^{(1)} - id_n^{(l)}\mathbf{N}_{e1n}^{(1)} + ia_n^{(l)}\mathbf{N}_{e1n}^{(3)} - b_n^{(l)}\mathbf{M}_{o1n}^{(3)}], \tag{1}$$

$$\mathbf{H}_l = -\frac{k_l}{\omega\mu}\sum_{n=1}^{\infty} E_n[d_n^{(l)}\mathbf{M}_{e1n}^{(1)} + ic_n^{(l)}\mathbf{N}_{o1n}^{(1)} - ib_n^{(l)}\mathbf{N}_{o1n}^{(3)} - a_n^{(l)}\mathbf{M}_{e1n}^{(3)}], \tag{2}$$

where $E_n = i^n E_0(2n + 1)/n(n + 1)$, ω is the angular frequency, and $\mathbf{M}_{o1n}^{(j)}$, $\mathbf{M}_{e1n}^{(j)}$, $\mathbf{N}_{o1n}^{(j)}$, and $\mathbf{N}_{e1n}^{(j)}$ ($j = 1, 3$) are the vector harmonic functions with the radial dependence $j_n(k_l r)$ for $j = 1$ and $h_n^{(1)}(k_l r)$ for $j = 3$.[7]

Following the treatment of Bohren and Huffman[7] for light scattering, we find that the internal EM fields ($\mathbf{E}_1$, $\mathbf{H}_1$) in the region $0 \le r \le r_1$ take the form[7,10]

$$\mathbf{E}_1 = \sum_{n=1}^{\infty} E_n[c_n^{(1)}\mathbf{M}_{o1n}^{(1)} - id_n^{(1)}\mathbf{N}_{e1n}^{(1)}], \tag{3}$$

$$\mathbf{H}_1 = -\frac{k_1}{\omega\mu}\sum_{n=1}^{\infty} E_n[d_n^{(1)}\mathbf{M}_{e1n}^{(1)} + ic_n^{(1)}\mathbf{N}_{o1n}^{(1)}]. \tag{4}$$

In the region outside the sphere, the total external fields are taken to be the superposition of the incident field and the scattered field, $\mathbf{E} = \mathbf{E}_i + \mathbf{E}_s$. According to Mie theory, the incident and scattered fields can be expanded by[7]

$$\mathbf{E}_i = \sum_{n=1}^{\infty} E_n[\mathbf{M}_{o1n}^{(1)} - i\mathbf{N}_{e1n}^{(1)}], \tag{5}$$

$$\mathbf{H}_i = -\frac{k}{\omega\mu}\sum_{n=1}^{\infty} E_n[\mathbf{M}_{e1n}^{(1)} + i\mathbf{N}_{o1n}^{(1)}], \tag{6}$$

$$\mathbf{E}_s = \sum_{n=1}^{\infty} E_n[ia_n\mathbf{N}_{e1n}^{(3)} - b_n\mathbf{M}_{o1n}^{(3)}], \tag{7}$$

$$\mathbf{H}_s = -\frac{k}{\omega\mu}\sum_{n=1}^{\infty} E_n[-ib_n\mathbf{N}_{o1n}^{(3)} - a_n\mathbf{M}_{e1n}^{(3)}]. \tag{8}$$

By comparing Eqs. (1) and (2), (3) and (4), and (5)–(8), one can deduce $a_n^{(1)} = b_n^{(1)} = 0$, $c_n^{(L+1)} = d_n^{(L+1)} = 1$, $a_n = a_n^{(L+1)}$, and $b_n = b_n^{(L+1)}$. The expansion coefficients $c_n^{(l)}$, $d_n^{(l)}$, $a_n^{(l)}$, and $b_n^{(l)}$ and scattering coefficients a_n, b_n are obtained by matching the tangential components of EM fields at each interface. From the boundary conditions, there are four independent linear equations in the aforementioned coefficients for a given n. In a traditional way, however, we have to solve the eight equations for the coefficients.[7,10,13] The details are given in Appendix A.

We define the following:

$$D_n^{(1)}(z) = \psi_n'(z)/\psi_n(z), \tag{9}$$

$$D_n^{(3)}(z) = \zeta_n'(z)/\zeta_n(z), \tag{10}$$

$$R_n(z) = \psi_n(z)/\zeta_n(z). \tag{11}$$

Equations (A2) in Appendix A can be easily solved for the coefficients $A_n^{(l+1)}$ and $B_n^{(l+1)}$. By use of the notations of Wu *et al.*,[11] a recursion algorithm can be developed in the following way:

$$A_n^{(1)} = 0, \qquad H_n^a(m_1x_1) = D_n^{(1)}(m_1x_1), \tag{12a}$$

$$H_n^a(m_lx_l) = \frac{R_n(m_lx_l)D_n^{(1)}(m_lx_l) - A_n^{(l)}D_n^{(3)}(m_lx_l)}{R_n(m_lx_l) - A_n^{(l)}}, \tag{12b}$$

$$A_n^{(l+1)} = R(m_{l+1}x_l)\frac{m_{l+1}H_n^a(m_lx_l) - m_1D_n^{(1)}(m_{l+1}x_l)}{m_{l+1}H_n^a(m_lx_l) - m_lD_n^{(3)}(m_{l+1}x_l)}. \tag{12c}$$

Similarly, if the refractive indices appearing as factors in the two terms are interchanged and $A_n^{(l+1)}$ is replaced by $B_n^{(l+1)}$, expressions defining $A_n^{(l+1)}$ automatically become expressions for $B_n^{(l+1)}$ ($l = 1, 2, \ldots, L$),[9,10] such that

$$B_n^{(1)} = 0, \qquad H_n^b(m_1x_1) = D_n^{(1)}(m_1x_1), \tag{13a}$$

$$H_n^b(m_lx_l) = \frac{R_n(m_lx_l)D_n^{(1)}(m_lx_l) - B_n^{(l)}D_n^{(3)}(m_lx_l)}{R_n(m_lx_l) - B_n^{(l)}}, \tag{13b}$$

$$B_n^{(l+1)} = R(m_{l+1}x_l)\frac{m_lH_n^b(m_lx_l) - m_{l+1}D_n^{(1)}(m_{l+1}x_l)}{m_lH_n^b(m_lx_l) - m_{l+1}D_n^{(3)}(m_{l+1}x_l)}. \tag{13c}$$

Thus, from the known values of $A_n^{(l)}$ and $B_n^{(l)}$ in the lth layer, the values of $A_n^{(l+1)}$ and $B_n^{(l+1)}$ in the $(l + 1)$th layer are calculated in succession for $l = 1, 2, \ldots, L$. The calculation starts in the core with the values $A_n^{(1)} = B_n^{(1)} = 0$, which results from initial conditions inside the core. The final coefficients in this series can be identified with the scattering coefficients a_n, b_n [see Eqs. (A4) in Appendix A], which are

$$a_n = A_n^{(L+1)} = \frac{[H_n^a(m_Lx_L)/m_L + n/x_L]\psi_n(x_L) - \psi_{n-1}(x_L)}{[H_n^a(m_Lx_L)/m_L + n/x_L]\zeta_n(x_L) - \zeta_{n-1}(x_L)}, \tag{14}$$

$$b_n = B_n^{(L+1)} = \frac{[m_LH_n^b(m_Lx_L) + n/x_L]\psi_n(x_L) - \psi_{n-1}(x_L)}{[m_LH_n^b(m_Lx_L) + n/x_L]\zeta_n(x_L) - \zeta_{n-1}(x_L)} \tag{15}$$

because $m_{L+1} = 1$, which corresponds to the region outside the sphere.

Table 1. Asymptotic Behavior of the Logarithmic Derivatives of Riccati–Bessel Functions $D_n^{(i)}(z)$ (i = 1, 2, 3) for a Large, Absorbing Particle[a]

n	$D_n^{(1)}(z)$	$D_n^{(2)}(z)$	$D_n^{(3)}(z)$
0	$(0.11449^{-15}, -0.10000^{+01})$	$(0.64966^{-69}, -0.10000^{+01})$	$(0.00000, 0.10000^{+01})$
1	$(0.74646^{-04}, -0.10000^{+01})$	$(0.74646^{-04}, -0.10000^{+01})$	$(-0.73809^{-04}, 0.10000^{+01})$
30	$(0.34764^{-01}, -0.99870)$	$(0.34764^{-01}, -0.99870)$	$(-0.34344^{-01}, 0.99912)$
50	$(0.95292^{-01}, -0.99935)$	$(0.95292^{-01}, -0.99935)$	$(-0.94022^{-01}, 0.10004^{+01})$
60	$(0.13645, -0.10019^{+01})$	$(0.13645, -0.10019^{+01})$	$(-0.13455, 0.10032^{+01})$
70	$(0.18439, -0.10070^{+01})$	$(0.17769, -0.10099^{+01})$	$(-0.18172, 0.10084^{+01})$
75	$(0.21070, -0.10107^{+01})$	$(0.41264^{-01}, -0.21076^{+01})$	$(-0.20762, 0.10122^{+01})$
80	$(0.23845, -0.10154^{+01})$	$(-0.20190, 0.10435^{+01})$	$(-0.23494, 0.10169^{+01})$
85	$(0.26752, -0.10210^{+01})$	$(-0.26343, 0.10223^{+01})$	$(-0.26357, 0.10225^{+01})$
90	$(0.29777, -0.10278^{+01})$	$(-0.29339, 0.10291^{+01})$	$(-0.29339, 0.10291^{+01})$
99	$(0.35481, -0.10426^{+01})$	$(-0.34969, 0.10437^{+01})$	$(-0.34969, 0.10437^{+01})$
116	$(0.46923, -0.10806^{+01})$	$(-0.46296, 0.10809^{+01})$	$(-0.46296, 0.10809^{+01})$
130	$(0.17656, -0.13895^{+01})$	$(-0.56047, 0.11206^{+01})$	$(-0.56047, 0.11206^{+01})$

[a]The refractive index is $m = 1.05 + 1i$, the size parameter is $x = 80$, and $N_{\text{stop}} = 116$.

The Riccati–Bessel functions $\psi_n(z)$ and $\zeta_n(z)$ satisfy the general recursive relations[10,14]

$$B_n(z) = (n/z)B_{n-1}(z) - B'_{n-1}(z), \tag{16}$$

$$B'_n(z) + (n/z)B_n(z) = B_{n-1}(z), \tag{17}$$

beginning with

$$\psi_{-1}(z) = \cos z, \qquad \psi_0(z) = \sin z,$$

$$\zeta_{-1}(z) = \cos z + i \sin z, \qquad \zeta_0(z) = \sin z - i \cos z.$$

The Riccati–Bessel function $B_n(z)$ represents $\psi_n(z)$ and $\zeta_n(z)$. From the two recurrence relations, the logarithmic derivatives of them satisfy an identical recurrence expression:

$$D_n^{(i)}(z) = [n/z - D_{n-1}^{(i)}(z)]^{-1} - n/z, \qquad i = 1, 3. \tag{18}$$

Of the many practical applications, the scattered fields in the far zone are of interest. Just like the treatment of Mie theory for a single homogeneous sphere,[7,11,13] once the scattering coefficients are calculated, the overall radiative properties of the composite particle are completely determined by the scattering coefficients a_n and b_n. Thus we can determine all the measurable quantities associated with scattering and absorption, i.e., the scattering, extinction, and backscatter efficiencies (Q_{sca}, Q_{ext}, and Q_{back}) and scattering amplitudes (S_1 and S_2), and the polarization degree P.

3. Computational Scheme: Recursive Algorithm

Although the computation appears to be straightforward, there are some pitfalls to be avoided. First, perhaps the worst of these occurs when the shell is a strongly absorbing particle such as soot aerosol. The case may lead to failure when one directly uses Aden and Kerker's equations, Bohren and Huffman's program, or Wu *et al.*'s method or expressions described above. The reason for this is that the numerator and denominator involve the subtraction of nearly equal terms, and the small round-off error will cause the results to be largely erroneous. In addition, the magnitude of a spherical Bessel function increases exponentially with the large complex argument and may easily exceed the limits of any computer if the particles are sufficiently large and absorbing.

However, for the scattering by a multilayered sphere, the recursive method, except for the numerical difficulties mentioned above, is a more convenient form for computation; in addition, the basic expressions [Eqs. (14) and (15)] have the same forms as those for a homogeneous sphere, which are the well-known Mie scattering coefficients. Then we still rely on the recursive method and modify the equations to remove the computational difficulties.

A. Behavior of Riccati–Bessel Functions

Wu and Wang[10] have discussed in detail the asymptotic form of logarithmic derivatives and ratios of Riccati–Bessel functions. However, as originally presented, these behaviors are suitable only for the case of a nonabsorbing or weakly absorbing sphere and do not provide enough information for the case of the large and strongly absorbing sphere. They found that real and imaginary parts of $\psi_n(z)/\chi_n(z)$ and $\psi_n(z)/\zeta_n(z)$ rapidly decrease to very small values close to zero. In addition, $D_n^2(z) = D_n^3(z) \approx -D_n^1(z)$ when $n > N_{\text{stop}}$, where N_{stop} will be discussed in Subsection 3.C. However, for the case of a large and highly absorbing sphere [i.e., large Im(z)], these functions behave different. Tables 1 and 2 present, as an example, the asymptotic behaviors of $D_n^{(i)}(z)$ (i = 1, 2, 3), $\psi_n(z)/\chi_n(z)$, and $\psi_n(z)/\zeta_n(z)$. The size parameter and refractive index in Tables 1 and 2 are $x = 80$, $m = (1.05, 1.0)$, respectively. When n is small (e.g., smaller than 60 in this case), we may find that $D_n^2(z) = D_n^1(z) \approx -D_n^3(z)$, the ratio $\psi_n(z)/\chi_n(z) \approx i$, and the ratio $\psi_n(z)/\zeta_n(z)$ is always big. It is clear that all these functions exhibit obviously different behaviors from the ones shown in Ref. 10. Only when n is very big, such as $n \gg N_{\text{stop}}$, are their behaviors the same as those described by Wu and Wang.[10] One can derive the equations for ratios $\psi_n(z)/\chi_n(z)$ and $\psi_n(z)/$

Table 2. Asymptotic Behavior of the Ratios of Riccati–Bessel Functions $\psi_n(z)/\chi_n(z)$ and $\psi_n(z)/\zeta_n(z)$ for a Large, Absorbing Particle[a]

n	$\psi_n(z)/\zeta_n(z)$	$\psi_n(z)/\chi_n(z)$
0	$(0.11533^{+69}, -0.15306^{+70})$	$(-0.64966^{-69}, 0.10000^{+01})$
1	$(-0.95073^{+68}, 0.15138^{+70})$	$(-0.11209^{-15}, 0.10000^{+01})$
30	$(0.32442^{+67}, -0.49140^{+67})$	$(0.26380^{-13}, 0.10000^{+01})$
40	$(0.48128^{+65}, 0.64583^{+65})$	$(0.27452^{-11}, 0.10000^{+01})$
60	$(0.89353^{+59}, 0.31796^{+60})$	$(0.35850^{-06}, 0.10000^{+01})$
70	$(0.91555^{+56}, -0.13547^{+56})$	$(0.34750^{-02}, 0.10008^{+01})$
75	$(0.29789^{+54}, -0.88309^{+54})$	$(0.18785, 0.15034^{+01})$
90	$(0.11275^{+48}, 0.42521^{+47})$	$(0.35158^{-06}, 0.96609^{-07})$
99	$(0.18051^{+43}, 0.81673^{+42})$	$(0.56667^{-11}, 0.19564^{-11})$
116	$(-0.86121^{+32}, -0.32339^{+31})$	$(-0.26037^{-21}, 0.14316^{-22})$
125	$(-0.85806^{+25}, 0.57128^{+26})$	$(-0.98922^{-29}, 0.17451^{-27})$
130	$(0.49007^{+22}, -0.12016^{+23})$	$(0.11408^{-31}, -0.37570^{-31})$

[a]The refractive index and the size parameter are the same as in Table 1.

$\zeta_n(z)$ by using the general recursive relations Eqs. (16)–(18) above, as follows,

$$\frac{\psi_n(z)}{\chi_n(z)} = \frac{\psi_{n-1}(z)}{\chi_{n-1}(z)} \frac{[D_n^{(2)}(z) + n/z]}{[D_n^{(1)}(z) + n/z]}, \tag{19}$$

$$\frac{\psi_n(z)}{\zeta_n(z)} = \frac{\psi_{n-1}(z)}{\zeta_{n-1}(z)} \frac{[D_n^{(3)}(z) + n/z]}{[D_n^{(1)}(z) + n/z]}, \tag{20}$$

with the starting ratios

$$\frac{\psi_0(z)}{\chi_0(z)} = i\,\frac{1 - \exp(2ai)\exp(-2b)}{1 + \exp(2ai)\exp(-2b)}, \tag{21}$$

$$\frac{\psi_0(z)}{\zeta_0(z)} = \frac{1 - \exp(-2ai)\exp(2b)}{2}, \tag{22}$$

where $z = m_l x_l = a + ib$. When the radius, r_l, is larger than the wavelength of light and the imaginary part of the refractive index of the shell is large [i.e., large Im(mx)], the value of $\psi_0(z)/\chi_0(z)$ is nearly equal to a complex constant i. Both the real and the imaginary parts of $\psi_0(z)/\zeta_0(z)$ become big. At this moment, the other algorithms, i.e., Aden and Kerker's and Bohren and Huffman's methods, will encounter the numerical difficulties. Likewise, for a large and strongly absorbing thin sphere, because of $D_n^1(z) = D_n^2(z)$ and $\psi_n(z)/\chi_n(z) \approx i$ (discussed above), Eqs. (19) and (21) of Wu *et al.*[11] are nearly equal to 0/0. The reason for this is that the numerator and denominator involve differences of terms, which are the subtraction of nearly equal quantities to obtain a small one, and result in numerically meaningless remainders. In addition to these problems, the magnitude of $\psi_0(z)/\zeta_0(z)$ increases exponentially with the complex argument; although the zero-order function might not exceed the limits of the computer, successive higher-order functions computed by upward recurrence might.

B. Recursive Algorithm

To remove these difficulties, Eqs. (12) and (13) should be rewritten in a form amenable to accurate calculation. We introduce a ratio $Q_n^{(l)}$, defined as

$$Q_n^{(l)} = \frac{R_n(z_1)}{R_n(z_2)} = \frac{\psi_n(m_l x_{l-1})}{\zeta_n(m_l x_{l-1})} \Big/ \frac{\psi_n(m_l x_l)}{\zeta_n(m_l x_l)}. \tag{23}$$

The presence of the ratio $Q_n^{(l)}$ is a characteristic of our recurrence expressions for scattering coefficients. Then Eqs. (12b) and (12c) are combined into one numerically stable form, namely,

$$H_n^a(m_l x_l) = \frac{G_2 D_n^{(1)}(m_l x_l) - Q_n^{(l)} G_1 D_n^{(3)}(m_l x_l)}{G_2 - Q_n^{(l)} G_1}. \tag{24}$$

As before, the determinant $H_n^b(m_l x_l)$ is obtained from $H_n^a(m_l x_l)$ by interchanging the positions of m_l and m_{l-1} and by the replacement of H_n^a with H_n^b. Thus

$$H_n^b(m_l x_l) = \frac{\tilde{G}_2 D_n^{(1)}(m_l x_l) - Q_n^{(l)} \tilde{G}_1 D_n^{(3)}(m_l x_l)}{\tilde{G}_2 - Q_n^{(l)} \tilde{G}_1}. \tag{25}$$

The other notations in Eqs. (24) and (25) for $l = 2, 3, \ldots, L$ are

$$G_1 = m_l H_n^a(m_{l-1} x_{l-1}) - m_{l-1} D_n^{(1)}(m_l x_{l-1}), \tag{26}$$

$$G_2 = m_l H_n^a(m_{l-1} x_{l-1}) - m_{l-1} D_n^{(3)}(m_l x_{l-1}), \tag{27}$$

$$\tilde{G}_1 = m_{l-1} H_n^b(m_{l-1} x_{l-1}) - m_l D_n^{(1)}(m_l x_{l-1}), \tag{28}$$

$$\tilde{G}_2 = m_{l-1} H_n^b(m_{l-1} x_{l-1}) - m_l D_n^{(3)}(m_l x_{l-1}). \tag{29}$$

Finally, the scattering coefficients, a_n and b_n, can be successfully computed by Eqs. (14) and (15) and (24) and (25). These equations constitute the basic expressions for calculating the scattering fields.

C. Computational Scheme

According to the above analysis, the calculation of scattering coefficients depends mainly on the logarithmic derivatives of Riccati–Bessel functions, $D_n^{(1)}(z)$ and $D_n^{(3)}(z)$. As discussed by Wiscombe,[16] the $D_n^{(1)}(z)$ can be accurately calculated for a large do-

main of complex argument by use of the downward recurrence. The number of terms, $N_{\max}$, in the partial-wave expansion is a function of the size parameters. Theory and experiment show that a good choice for the number of terms is given by $N_{\max} = \max(N_{\text{stop}}, |m_l x_l|, |m_l x_{l-1}|) + 15$, $l = 1, 2, \ldots, L$. The value of N_{stop} is the integer closest to

$$N_{\text{stop}} = \begin{cases} x_L + 4x_L^{1/3} + 1 & 0.02 \le x_L \le 8 \\ x_L + 4.05x_L^{1/3} + 2 & 8 \le x_L \le 4200 \\ x_L + 4x_L^{1/3} + 2 & 4200 \le x_L \le 20{,}000 \end{cases}; \tag{30}$$

these criteria were discussed by Wiscombe.[16] The logarithmic derivative $D_n^{(3)}(z)$ is calculated by a new upward recurrence discussed in Ref. 13, and recurrence is begun with

$$D_0^{(3)}(z) = i, \tag{31}$$

$$\psi_0(z)\zeta_0(z) = \tfrac{1}{2}[1 - (\cos 2a + i \sin 2a)\exp(-2b)], \tag{32}$$

where $z = a + ib$. Mackowski *et al.*[13] found that this method of computing $D_n^{(3)}(z)$ was stable for all values of z, as opposed to some methods of upward recurrence,[8–10,12] which could become unstable for relatively small $\text{Im}(z)$. As we will see, this is the reason why the Toon and Ackerman[8] and the Bhandari[9] methods cannot guarantee $Q_{\text{ext}} = Q_{\text{sca}}$ for a large nonabsorbing sphere. The ratio $Q_n^{(l)}$ is calculated by use of upward recursion. By using the general relations, we can write

$$Q_n^{(l)} = Q_{n-1}^{(l)} \frac{\lfloor D_n^{(3)}(z_1) + n/z_1 \rfloor}{\lfloor D_n^{(1)}(z_1) + n/z_1 \rfloor} \Bigg/ \frac{\lfloor D_n^{(3)}(z_2) + n/z_2 \rfloor}{\lfloor D_n^{(1)}(z_2) + n/z_2 \rfloor}, \tag{33}$$

with the starting ratio

$$Q_0^{(l)} = \frac{R_0(z_1)}{R_0(z_2)} = \frac{\exp(-i2a_1) - \exp(-2b_1)}{\exp(-i2a_2) - \exp(-2b_2)} \times \exp[-2(b_2 - b_1)], \tag{34}$$

where $z_1 = m_l x_{l-1} = a_1 + ib_1$, $z_2 = m_l x_l = a_2 + ib_2$. From Table 2 or Eq. (22), we found the values of $R_n(z_1)$ and $R_n(z_2)$ will be $\gg 1$ for large $\text{Im}(mx)$ and can conceivably result in overflow, so they are all not bounded. The ratio, $Q_n^{(l)}$, of these two functions, however, is always bounded because $b_2 > b_1$. Alternatively, by use of the recursive relation (18), the ratio $Q_n^{(l)}$ gives

$$Q_n^{(l)} = Q_{n-1}^{(l)} \left(\frac{x_{l-1}}{x_l}\right)^2 \frac{[z_2 D_n^{(1)}(z_2) + n]}{[z_1 D_n^{(1)}(z_1) + n]} \frac{[n - z_2 D_{n-1}^{(3)}(z_2)]}{[n - z_1 D_{n-1}^{(3)}(z_1)]}. \tag{35}$$

Note that the variable $Q_n^{(l)}$ and its form that we obtained by using Eq. (33) or (35) are different from those employed by other algorithms. When n is large compared with the size parameters in question, the ratio, $Q_n^{(l)}$, approaches zero rapidly. Particularly, the errors in evaluating $Q_n^{(l)}$ do not propagate and grow when n increases. For example, the ratio $Q_n^{(l)}$ behaves as $(x_1/x_2)^{2n}$ for a two-layered sphere when $n \gg x_2$. This has the consequence that, for such large values of n, the scattering coefficients reduce to the Mie coefficients that correspond to a homogeneous sphere with the parameters m_2 and x_2. For $x_1 \ll x_2$ (a tiny core), a less stringent condition, $n \gg x_1$, is enough.[9] Furthermore, in the event that for $(x_2 - x_1) \ll 1$ (a thin shell[17] or a finely stratified sphere[14]), the ratio $Q_n^{(l)}$ varies little and approximates a constant with the n increasing. Then we can see that this recursive formula is numerically stable, as the fractional errors do not grow with n.[8,9]

The final terms to be computed are $\psi_n(x_L)$ and $\zeta_n(x_L)$. These are Riccati–Bessel functions of real argument and are therefore bounded. Thus the two functions are calculated by use of upward recursion in the same way as in Mie theory.[8,16]

4. Tests of the Algorithms and Results

To examine how this recursive algorithm works, we have calculated the extinction efficiency, scattering efficiency, and other scattering-related quantities associated with the external field for various size and refractive indices. Several comparisons are made with calculations performed by other algorithms and with the published results for quite different cases. All the calculations are performed with double-decision arithmetic.

A. Other Algorithms

We first performed various tests for the scattering, extinction, and backscattering efficiencies (Q_{sca}, Q_{ext}, Q_{back}) by comparing them with the corresponding values of other methods for a two-layered sphere system. First, the comparisons are performed when the imaginary parts of $m_l x_l$ or $m_l x_{l-1}$ are relatively small (e.g., do not exceed 30, as suggested by Bohren and Huffman[7]). The results show good agreement in all instances with the values from the methods of Toon and Ackerman,[8] Bhandari,[9] Wu *et al.*,[11] and Bohren and Huffman.[7] Second, the comparisons are performed for the case of the large and strongly absorbing coated sphere, such as when soot forms a thin shell on the outside of a nonabsorbing (a water droplet) or weakly absorbing (sulfate aerosol) sphere. We find that the code of Bohren and Huffman[7] cannot perform this calculation. The method of Wu *et al.*[11] may be subject to some numerical difficulties. Whereas the first two algorithms and ours do not encounter the numerical problems, the results show agreement even for this difficult case that could cause other algorithms to fail. As an illustration, the comparison of different algorithms for the scattering and extinction efficiencies and the single-scattering albedo is shown in Fig. 2. This example is a water droplet ($m_1 = 1.33 + i0.00$) on which the soot ($m_2 = 1.59 + i0.66$) has formed a thin shell; it is opposed to Fig. 5 in Wu and Wang[10]; the volume fraction of soot

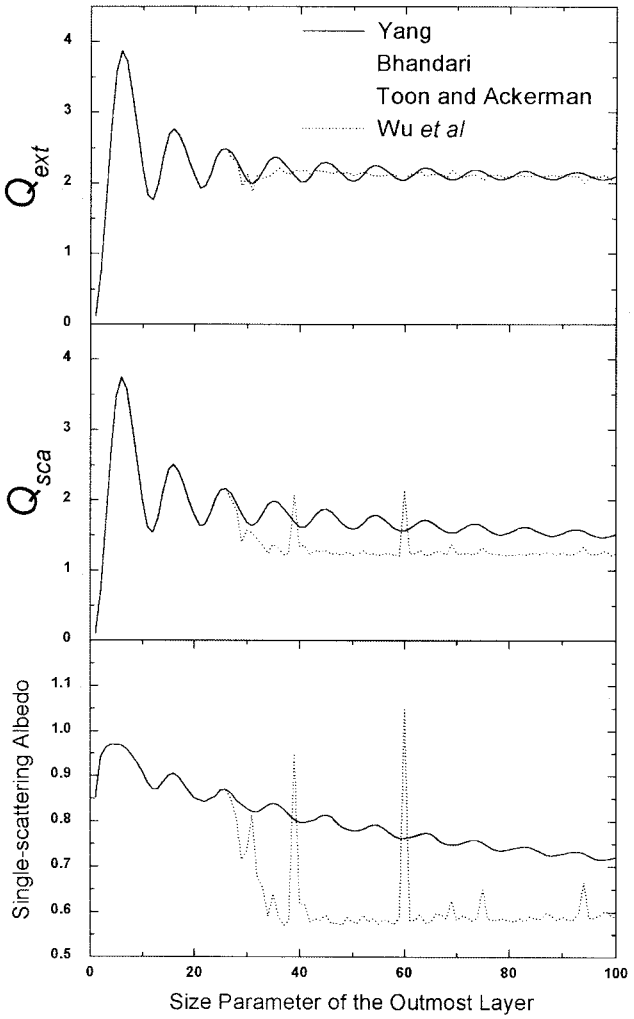

Fig. 2. Extinction and scattering efficiencies (Q_{ext}, Q_{sca}) and single-scattering albedo as a function of the size parameter of the outmost layer for a soot-coated water sphere. A comparison of the results obtained from Wu *et al.*,[11] Bhandari,[9] and Toon and Ackerman[8] is shown. The refractive indices of water and soot are $m_1 = 1.33 + i0.00$, $m_2 = 1.59 + i0.66$, respectively. The volume fraction of soot is 0.01.

here is equal to 0.01. We see in Fig. 2 that the results of Wu *et al.*[11] are obviously unreasonable when the size parameter is larger than 30. Finally, if the sphere is large and nonabsorbing, the algorithms of Toon and Ackerman[8] and Bhandari[9] also cannot guarantee $Q_{ext} = Q_{sca}$ because of the use of unstable upward recurrence for $D_n^{(3)}(z)$. From our practice, this deficiency can be remedied by application of the new upward recurrence[13] for $D_n^{(3)}(z)$. Furthermore, to compare the algorithm's efficiency, we show the computational domain (number of layers versus the size parameter) in Fig. 3, where the refractive index and the size parameter are the same as those in Ref. 11. Figure 3 demonstrates that our method can also increase the affordable number of layers and the size parameter by several orders of magnitude. This limit is due only to the memory of the computer.

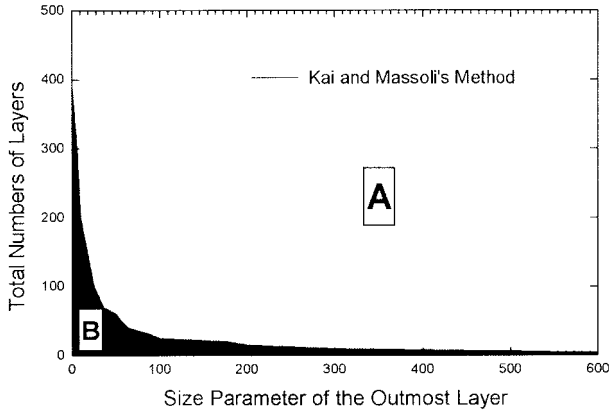

Fig. 3. Computational domain for a multilayered sphere. The solid curve is the affordable number of layers, and region B is the computational domain obtained by Kai and Massoli.[14] Region A is the computational domain of our algorithm. The refractive index $m_l = n_l + ik_l$ is $n_l = n_1 + 0.5(n_L - n_1)(1 - \cos t\pi)$, and $k_l = 0$, where $t = (l - 1)/(L - 1)$, $n_1 = 1.01n_L$, and $n_L = 1.33$. The size parameter is $x_l = x_1 + t(x_L - x_1)$, where $l = 1, 2, \ldots, L$, $x_1 = 0.001x_L$, and L is the total number of layers.

We also checked results for extinction efficiency factors by comparing them with the tabulated values of Espenscheid *et al.*[18] for real refractive indices, a size parameter of 10 for the total particle, and a large range of core sizes. There is good agreement to four decimal digits that were reported by Ref. 18. We also performed several tests, all of which are correct in comparison with Mie theory (Mie code was provided by Wiscombe) to at least six decimal digits, for various efficiency factors and an asymmetry parameter. These tests include setting the refractive indices of the core and shell equal to each other, setting the refractive index of the shell equal to that of free space ($1 + 0i$), setting the radius core and shell equal to each other, and setting the core radius to zero.

B. Kai and Massoli Model

As in Kai and Massoli,[14] the radial profile of the refractive index, $m_l = n_l + ik_l$, is described at the lth-layer level by $n_l = n_1 + 0.5(n_L - n_1)(1 - \cos t\pi)$ and $k_l = 0$, where $t = (l - 1)/(L - 1)$, $n_1 = 1.43$, and $n_L = 1.33$. The size parameter is $x_l = x_1 + t(x_L - x_1)$, $l = 1, 2, \ldots, L$, and L is the total number of layers. Figure 4 displays the scattering efficiency (Q_{sca}) as a function of dimensionless core size parameter x_1/x_L. We found that our results are in good accord with the graphic results of Kai and Massoli (see their Fig. 4).[14] Therefore, as pointed out by Wu *et al.*,[11] it is not necessary to use the Taylor expansions for the ratios of the Riccati–Bessel function. The numerical results do not exhibit so-called second-kind or third-kind round-off errors, as mentioned by Kai and Massoli.[14] In Fig. 5 the vertically polarized intensity $i_\perp$ is plotted against the scattering angle θ. As shown, the present formulations yield results in agreement with Fig. 6 of Kai and Massoli for two different cases.[14] In this stratified sphere model, for case 1, $m_l = x_L/x_l$, and, for case 2, $m_l = 1.01(x_L/x_l)^2$,

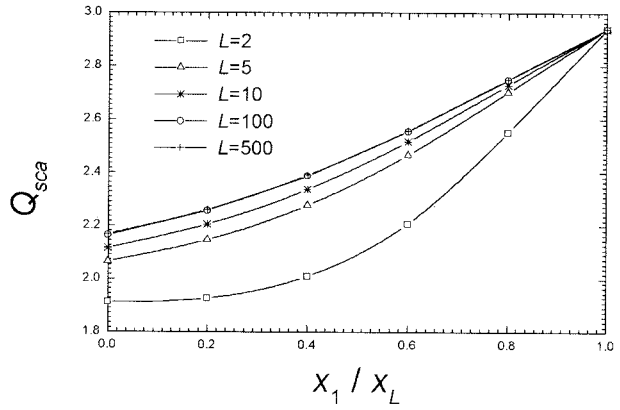

Fig. 4. Scattering efficiency Q_{sca} versus the dimensionless size parameter of the core x_1/x_L. The refractive index $m_l = n_l + ik_l$ is $n_l = n_1 + 0.5(n_L - n_1)(1 - \cos t\pi)$, and $k_l = 0$, where $t = (l - 1)/(L - 1)$, $n_1 = 1.43$, and $n_L = 1.33$. The size parameter is $x_l = x_1 + t(x_L - x_1)$, $l = 1, 2, \ldots, L$, and L is the total number of layers.

where $L = 1500$ and $x_l = x_1 + (x_L - x_1)(l - 1)/(L - 1)$. As the total number of layers become large enough, the estimated values by a multilayered sphere are in good agreement with the analytic solutions. Therefore the multilayered sphere model can be used to describe all types of radially inhomogeneous sphere, and the converged solutions of the multilayered sphere model can be considered to be the true solutions of realistic radially inhomogeneous spheres, to a good approximation.[14]

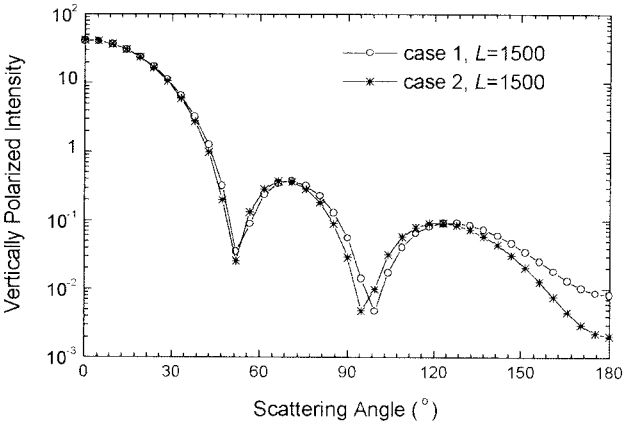

Fig. 5. Vertically polarized intensity $i_\perp$ as a function of the scattering angle θ for a radially multilayered sphere with a size parameter $x_L = 5$. The refractive indices in the lth layer, are, for case 1, $m_1 = 1.0834 + i0.0$, $m_l = x_L/x_l$, and, for case 2, $m_1 = 1.0779 + i0.0$, $m_l = 1.01(x_L/x_l)^2$. The size parameter is $x_l = x_1 + (x_L - x_1)(l - 1)/(L - 1)$, where the total number of layers is $L = 1500$.

C. Mackowski *et al*. Model

For the purposes of illustration, the particular type of particle considered here consists of a mixture of absorbing, sub-micro-sized particles suspended in a droplet of water. Such a mixture has relevance to droplet combustion of solid fuel and water slurries.[13] The mixture is assumed to be characterized by a radially dependent effective refractive index, m_{eff}, reading as [see Eq. (72) of Mackowski *et al*.[13]]

$$m_{\text{eff}}^2(r) = m_{\text{med}}^2\left\{1 + 3f_v(r)\,\frac{\beta}{[1 - f_v(r)\beta]}\right\}, \quad (36)$$

where $\beta = (m_{\text{abs}}^2 - m_{\text{med}}^2)/(m_{\text{abs}}^2 + 2m_{\text{med}}^2)$, m_{med} is the refractive index of the water medium, m_{abs} is the refractive index of the absorbing particle, and $f_v(r)$ is the volume fraction of the absorbing particle. Following Mackowski *et al*.'s treatment,[13] five cases of distributions of $f_v(r)$ are calculated. They are (1) a uniform distribution, $f_v(r) = \bar{f}_v = 0.1$; (2) a two-layered sphere with the absorbing material existing as the core, $x_1 = \bar{f}_v^{1/3} x_L$; (3) a two-layered sphere with the absorbing material forming the shell, $x_1 = (1 - \bar{f}_v)^{1/3} x_L$; (4) the absorbing material distributed according to $f_v(x) = 4/3(x/x_L)\bar{f}_v$; and (5) the absorbing material distributed according to $f_v(x) = 1/4(1 - x/x_L)\bar{f}_v$.

The effect of absorbing material distributions on the overall radiative properties, i.e., Q_{sca}, Q_{ext}, and Q_{back}, are given in Table 3. These results agree almost exactly with the values calculated by Mackowski *et al*.[13] The only minor difference is the value of Q_{back} in the second line of Table 3. The effect of the distribution of absorbing material has little influence on the overall extinction efficiency of the particle, but the scattering efficiency is greatest for core absorption and smallest for uniformly distributed absorption. Also, the single-scattering albedo ϖ behaves quite differently. It should be particularly pointed out that other algorithms could encounter numerical difficulties when they are used with case 3.

D. Bhandari Model

To have a comparison with the results of Bhandari,[17] we considered the absorption of visible light by tiny soot particle forming the core of a water droplet.

Table 3. Extinction, Scattering, and Backscattering Efficiencies and Single-Scattering Albedo (Q_{ext}, Q_{sca}, Q_{back} and ϖ)[a]

Cases	Q_{ext}	Q_{sca}	Q_{back}	ϖ
1: $f_v(x) = \text{const} = \bar{f}_v$	2.08977	1.11664	0.03005	0.534339
2: core absorption	2.20718	1.87320	2.61685	0.848686
3: shell absorption	2.09947	1.29372	0.19948	0.616211
4: $f_v(x) = 4/3x/x_L\bar{f}_v$	2.08933	1.12213	0.03399	0.537076
5: $f_v(x) = 1/4\ (1 - x/x_L)\bar{f}_v$	2.09958	1.28749	0.17248	0.613213

[a] $m_{\text{med}} = 1.33 + 0i$, $m_{\text{abs}} = 2 + 1i$, $x_L = 100$, and volume fraction $\bar{f}_v = 0.1$.

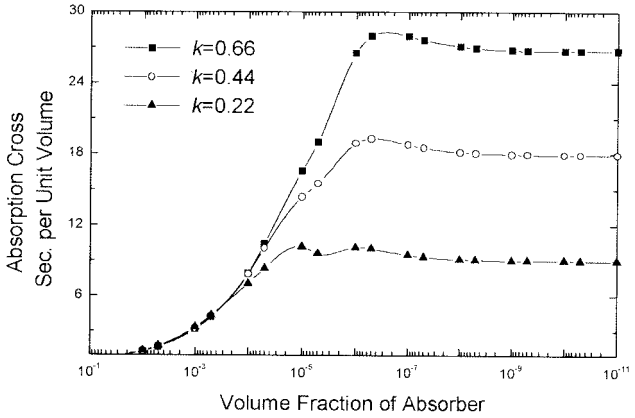

Fig. 6. Absorption cross section per unit volume of absorbing material, σ_{abs}/V, as a function of its volume fraction f_v for a two-layer sphere model with a radius $r_2 = 5$ μm at the outer rim. The refractive index of the water shell is $m_2 = 1.33 + i0.00$, and that of the absorbing core is $m_1 = 2.0 + ik$, where $k = 0.22, 0.44, 0.66$. The case of $k = 0.66$ corresponds to a soot particle. The wavelength is $\lambda = 0.5$ μm.

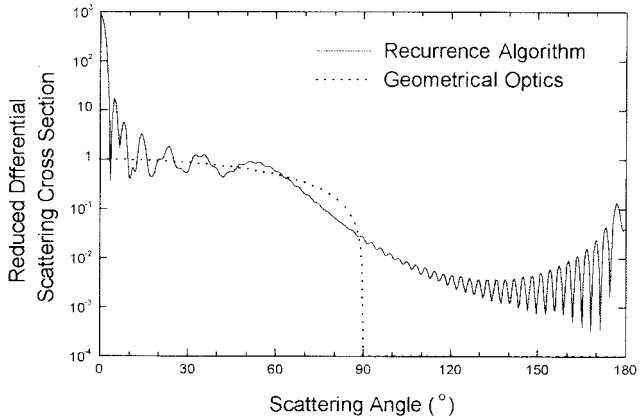

Fig. 8. Reduced differential cross section $d\sigma/d(a^2\Omega)$ as a function of scattering angle θ for a spherical Luneburg lens with a size parameter $x_L = 60$. The size parameter in the lth layer is $x_l = lx_L/500$. The refractive index is $m_l = [2 - (\bar{x}/x_L)^2]^{1/2}$, with $\bar{x} = (\bar{x}_{l-1} + \bar{x}_l)/2$, for $l = 2, 3, \ldots, L$. For the geometrical optics theory, $d\sigma/d\Omega = a^2 \cos(\theta)$.

This is one of the cases of practical interest in the study of scattering of light by polluted clouds and fog. For the calculation, $r_2 = 5$ μm, $\lambda = 0.5$ μm, m_2 (water) $= 1.33 + i0.00$, and $m_1 = 2.0 + ik$. For the special case of soot, take $k = 0.66$. The other values of k are set to 0.22 and 0.44. The absorption cross section per unit volume of absorbing material, σ_{abs}/V, is plotted against the volume fraction f_v of the absorbing material for different values of k in Fig. 6. For the sake of illustration, we consider again the case of a water droplet ($m_1 = 1.33 + i0.00$) with the soot ($m_2 = 2.0 + i0.66$) forming a thin shell on the outside. The results are shown in Fig. 7. As can be seen, the different distributions of the soot in a water droplet (i.e., the soot existing as the core or shell) profoundly affect the absorption cross section per unit volume of the absorbing material. The graphical results agree well with those computed by a perturbative approximation method.[17] More important, other algorithms could suffer from numerical difficulties in the case when the soot exists as a thin shell. This agreement is also a good test of the numerical stability of the computational procedure outlined in Section 3.

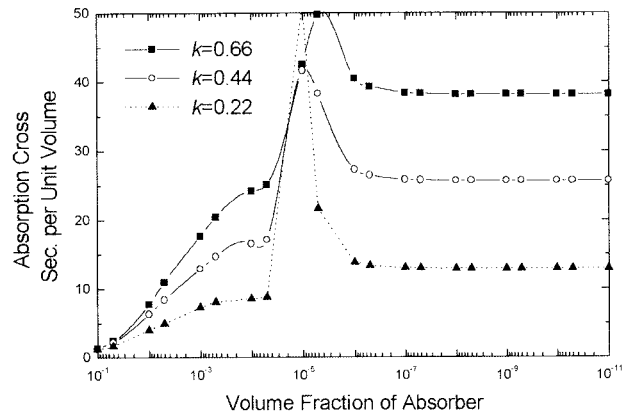

Fig. 7. As in Fig. 6, but the absorbing material in the two-layer sphere model exists as a thin shell on the outside of a water droplet.

E. Luneburg Lens

This test case is the scattering from a spherical Luneburg lens, which is also approximated as a multilayered sphere. The Luneburg lens is characterized by a refractive index that varies according to the relation[12]

$$m(r) = [2 - (r/a)^2]^{1/2}, \tag{37}$$

where a is the radius of the outer rim of the spherical lens and r is the radial distance measured from the center. The refractive index is a radially varying continuous profile. The radially multilayered sphere model may be used not only to calculate spheres with discontinuous profiles of refractive index but also to approximate spheres with continuous profiles of refractive index by use of a large number of layers. In the present calculation, the Luneburg lens is modeled as a multilayered sphere with 500 layers. The refractive index of each layer is defined to be equal to $m(r)$ at the midpoint of the layer, i.e., $m_l = m(\bar{r})$, $\bar{r} = (r_{l-1} + r_l)/2$ for $l = 2, 3, \ldots, L$. The size parameter is obtained when the sphere is divided into 500 equally spaced layers.[12] According to geometrical optics theory, the differential cross section can be expressed as[12]

$$d\sigma/d\Omega = a^2 \cos(\theta). \tag{38}$$

Results of our procedure are shown in Fig. 8 for size parameter $x_L = 60$. The quantity plotted is the reduced differential cross sections $d\sigma/d(a^2\Omega)$ (i.e., the differential cross section divided by a^2). Comparisons are made with the calculations performed previously by Johnson[12] for the situation of a

multilayered sphere model and geometrical optics theory. As a further test, when we compare results with those plotted in Fig. 3 of Johnson,[12] it can be seen that there was good agreement in all instances.

5. Summary and Conclusions

An improved and more efficient algorithm for scattering coefficients of a multilayered sphere has been presented. The procedures include three operations. First, the derivation is based on the physical consideration: The internal and external EM fields are considered a superposition of two kinds of wave: inward and outward waves. The radial dependence of the inward wave is governed by the first kind of spherical Bessel function $j_n(kr)$. In contrast, the radial dependence of the outward wave is governed by the first kind of spherical Hankel function $h_n^{(1)}(kr)$. The final recursive expressions are similar in form to those of Mie theory for a homogeneous sphere. No special restriction on the number of layers is imposed by this method. More specially, this recursive algorithm is concise and convenient for program coding. Second, the Riccati–Bessel functions, ψ_n and ζ_n, are replaced with their logarithmic derivatives. This technique, long used in Mie theory and for coated spheres, circumvents the exponential dependence of the functions on the size parameter. Finally, a suitable ratio of Riccati–Bessel functions is bounded as the core size becomes small or as the size parameter becomes large. Presence of the ratio $Q_n^{(l)}$ is one of the characteristics of our recurrence expressions for scattering coefficients. The round-off errors that prevented previous algorithms from dealing with problems of highly absorbing and finely stratified spheres or large nonabsorbing stratified spheres have been eliminated. With those operations, the final recursive algorithm avoided the numerical difficulties in earlier methods that were due to the subtraction of nearly equal terms, leaving a small residual. The various tests show the recursive algorithm is numerically stable and correct for a large range of size parameters and refractive indices. This behavior contrasts with that of some other recurrence algorithms for solving highly absorbing thin-shell sphere problems, which could be subject to relatively severe round-off errors.

Appendix A: Boundary Conditions at the Interfaces

Following Bohren and Huffman's treatment,[7] we can expand the problem of scattering by a coated sphere into the problem of scattering by a multilayered sphere. The boundary conditions for different interfaces are

$$(\mathbf{E}_{l+1} - \mathbf{E}_l) \times \hat{\mathbf{e}}_r = 0, \qquad (\mathbf{H}_{l+1} - \mathbf{H}_l) \times \hat{\mathbf{e}}_r = 0, \quad \text{(A1)}$$

where $r = r_l$ and $l = 1, 2, \ldots, L-1, L$.

From the orthogonality, together with the field expansions, Eqs. (1)–(8), and the expressions for vector harmonics [Bohren and Huffman,[7] Eq. (4.50)], the boundary conditions above yield four independent linear equations in expansion coefficients $c_n^{(l)}$, $d_n^{(l)}$, $a_n^{(l)}$, $b_n^{(l)}$:

$$\begin{aligned}
&d_n^{(l+1)} m_1 \psi_n'(m_{l+1}x_l) - a_n^{(l+1)} m_l \zeta_n'(m_{l+1}x_l) \\
&\qquad - d_n^{(l)} m_{l+1} \psi_n'(m_l x_l) + a_n^{(l)} m_{l+1} \zeta_n'(m_l x_l) = 0, \\
&c_n^{(l+1)} m_l \psi_n(m_{l+1}x_l) - b_n^{(l+1)} m_l \zeta_n(m_{l+1}x_l) \\
&\qquad - c_n^{(l)} m_{l+1} \psi_n(m_l x_l) + b_n^{(l)} m_{l+1} \zeta_n(m_l x_l) = 0, \\
&c_n^{(l+1)} \psi_n'(m_{l+1}x_l) - b_n^{(l+1)} \zeta_n'(m_{l+1}x_l) \\
&\qquad - c_n^{(l)} \psi_n'(m_l x_l) + b_n^{(l)} \zeta_n'(m_l x_l) = 0, \\
&d_n^{(l+1)} \psi_n(m_{l+1}x_l) - a_n^{(l-1)} \zeta_n(m_{l+1}x_l) \\
&\qquad - d_n^{(l)} \psi_n(m_l x_l) + a_n^{(l)} \zeta_n(m_l x_l) = 0, \quad \text{(A2)}
\end{aligned}$$

where the Riccati–Bessel functions are $\psi_n(z) = z j_n(z)$ and $\zeta_n(z) = z h_n^{(1)}$. Let $A_n^{(l)} = a_n^{(l)}/d_n^{(l)}$ and $B_n^{(l)} = b_n^{(l)}/c_n^{(l)}$. In the core ($l = 1$), $a_n^{(1)}$ and $b_n^{(1)}$ must be zero because no outward fields exist in the region $r < r_1$ [see Eqs. (3) and (4)], which is different from the traditional treatment[7,10,13]; then we get $A_n^{(1)} = B_n^{(1)} = 0$. The auxiliary arguments $A_n^{(l)}$ and $B_n^{(l)}$, where $l = 2, 3, \ldots, L-1, L$, are easily obtained when the set of linear equations (A2) is solved.

For the outermost layer $r_l = r_L$, the external fields are

$$\begin{aligned}
\mathbf{E}_{L+1} &= \mathbf{E}_i + \mathbf{E}_s, \\
\mathbf{H}_{L+1} &= \mathbf{H}_i + \mathbf{H}_s. \quad \text{(A3)}
\end{aligned}$$

Thus, from Eqs. (1) and (2) and (5)–(8), we have $c_n^{(L+1)} = d_n^{(L+1)} = 1$, $a_n = a_n^{(L+1)} = A_n^{(L+1)}$, and $b_n = b_n^{(L+1)} = B_n^{(L+1)}$. For the sake of clearness, an alternative form of the set of Eqs. (A2) can be rewritten as

$$\begin{aligned}
&m_L \psi_n'(x_L) - a_n m_L \zeta_n'(x_L) - d_n^{(L)} \psi_n'(m_L x_L) \\
&\qquad + a_n^{(L)} \zeta_n'(m_L x_L) = 0, \\
&m_L \psi_n(x_L) - b_n m_L \zeta_n(x_L) - c_n^{(L)} \psi_n(m_L x_L) \\
&\qquad + b_n^{(L)} \zeta_n(m_L x_L) = 0, \\
&\psi_n'(x_L) - b_n \zeta_n'(x_L) - c_n^{(L)} \psi_n'(m_L x_L) + b_n^{(L)} \zeta_n'(m_L x_L) = 0, \\
&\psi_n(x_L) - a_n \zeta_n(x_L) - d_n^{(L)} \psi_n(m_L x_L) + a_n^{(L)} \zeta_n(m_L x_L) = 0 \\
&\qquad \text{(A4)}
\end{aligned}$$

because $m_{L+1} = 1$, which corresponds to the region outside the sphere.

The author thanks very specially the two anonymous reviewers for their comments and suggestions, which improved the presentation of our method. The author also appreciates our computer center and Wu-Zhou Wei for providing the use of the computer. This research was supported in part by Chinese Academy of Sciences (KZCX2-201), by the Coordinated Enhanced Observing Period Asia-Australia Monsoon Project on Tibetan Plateau (CAMP/Tibet), and by the National Natural Science Foundation of China (Grant 40275003).

References

1. M. Kerker, *The Scattering of Light and Other Electromagnetic Radiation* (Academic, New York, 1969).
2. P. Chylek, V. Ramaswamy, and R. J. Cheng, "Effect of graphitic carbon on the albedo of clouds," J. Atmos. Sci. **41,** 3076–3084 (1984).
3. J. V. Martins, P. Artaxo, C. Liousse, J. S. Reid, P. V. Hobbs, and Y. J. Kaufman, "Effects of black carbon content, particle size, and mixing on the light absorption by aerosols from biomass burning in Brazil," J. Geophys. Res. **103,** 32041–32050 (1998).
4. G. W. Kattawar and D. A. Hood, "Electromagnetic scattering from a spherical polydispersion of coated spheres," Appl. Opt. **15,** 1996–1999 (1976).
5. A. L. Aden and M. Kerker, "Scattering of electromagnetic waves from two concentric spheres," J. Appl. Phys. **22,** 1242–1246 (1951).
6. R. W. Fenn and H. Oser, "Scattering properties of concentric soot–water spheres for visible and infrared light," Appl. Opt. **4,** 1504–1509 (1965).
7. C. F. Bohren and D. R. Huffman, *Absorption and Scattering of Light by Small Particles* (Wiley, New York, 1983).
8. O. B. Toon and T. P. Ackerman, "Algorithms for the calculation of scattering by stratified spheres," Appl. Opt. **20,** 3657–3660 (1981).
9. R. Bhandari, "Scattering coefficients for a multilayered sphere: analytic expressions and algorithms," Appl. Opt. **24,** 1960–1967 (1985).
10. Z. S. Wu and Y. P. Wang, "Electromagnetic scattering for multilayered sphere: recursive algorithms," Radio Sci. **26,** 1393–1401 (1991).
11. Z. S. Wu, L. X. Guo, K. F. Ren, G. Gouesbet, and G. Grehan, "Improved algorithm for electromagnetic scattering of plane waves and shaped beams by multilayered sphere," Appl. Opt. **36,** 5188–5198 (1997).
12. B. R. Johnson, "Light scattering by a multilayer sphere," Appl. Opt. **35,** 3286–3296 (1996).
13. D. W. Mackowski, R. A. Altenkirch, and M. P. Menguc, "Internal absorption cross sections in a stratified sphere," Appl. Opt. **29,** 1551–1559 (1990).
14. L. Kai and P. Massoli, "Scattering of electromagnetic-plane waves by radially inhomogeneous spheres: a finely stratified sphere model," Appl. Opt. **33,** 501–511 (1994).
15. K. A. Fuller, "Scattering and absorption cross sections of compounded spheres. III. Spheres containing arbitrary located spherical inhomogeneities," J. Opt. Soc. Am. A **12,** 893–904 (1995).
16. W. J. Wiscombe, "Improved Mie scattering algorithms," Appl. Opt. **19,** 1505–1509 (1980).
17. R. Bhandari, "Tiny core or thin layer as a perturbation in scattering by a single-layered sphere," J. Opt. Soc. Am. A **3,** 319–328 (1987).
18. W. F. Espenscheid, E. Willis, E. Matijevic, and M. Kerker, "Aerosol studies by light scattering. IV. Preparation and particle size distribution of aerosol consisting of concentric spheres," J. Colloid Sci. **20,** 501–521 (1965).